

# An Eclipse-Balloon Study of Shadow Bands During the April 2024 Total Eclipse

Giana Deskevich<sup>a</sup>, Norris Bach<sup>b</sup>, Kristian Borysiak<sup>a</sup>, Russell J. Clark<sup>a</sup>, Louis W. Coban<sup>a,c</sup>, Istvan Danko<sup>a</sup>, Luke Docherty<sup>a</sup>, Michael Hatridge<sup>a</sup>, Howard Malc<sup>a</sup>, Boris Mestis<sup>a</sup>, Emma Moran<sup>a</sup>, Mathilda Nilsson<sup>a</sup>, Jeffrey B. Peterson<sup>b</sup>, Edward Michael Potosky<sup>a,c</sup>, Sandhya M. Rao<sup>a</sup>, Peri Schindelheim<sup>a</sup>, James D. Turnshek<sup>d</sup>, Ameya Velankar<sup>a</sup>, Ryan Young<sup>a</sup> and David A. Turnshek<sup>a,c</sup>

<sup>a</sup>Department of Physics and Astronomy, University of Pittsburgh, Pittsburgh, PA 15260, USA

<sup>b</sup>Department of Physics, Carnegie Mellon University, Pittsburgh, PA 15251, USA

<sup>c</sup>Allegheny Observatory, 159 Riverview Ave, University of Pittsburgh, Pittsburgh, PA 15214, USA

<sup>d</sup>Formant, San Francisco, CA 94105, USA

## ARTICLE INFO

### Keywords:

Total solar eclipse  
shadow bands  
atmospheric turbulence  
planetary boundary layer  
high-altitude balloons  
radiosondes  
spectrogram analysis  
optical phenomena  
light intensity measurements  
diffraction-interference

## ABSTRACT

In this study we searched for shadow bands associated with the total solar eclipse of April 8, 2024. Our aim was to improve our understanding of their origin. Shadow bands are debated to arise either from atmospheric turbulence within Earth's planetary boundary layer (PBL) or from a diffraction-interference effect occurring above the atmosphere. To test these theories, high altitude balloons (HABs) equipped with light sensors, similar ground light sensors, radiosondes launched with weather balloons, and an aircraft-mounted light sensor were deployed. Our team was located in Concan, TX, except for the plane which flew to NE Vermont to find clear weather. Unlike Pitt's 2017 HAB study, which detected a 4.5 Hz signal attributed to shadow bands above the PBL and on the ground, no shadow bands were detected above the PBL in Texas or in northeast Vermont, despite the use of improved instrumentation. Cloud cover prevented useful ground based measurements in Texas, limiting our conclusions about the nature of shadow bands. These findings suggest that shadow bands may not always be present or, if they are, may be primarily due to atmospheric turbulence. The results of this study and Pitt's 2017 study emphasize the need for future work.

## 1. Introduction

This paper presents an analysis of a search for shadow bands during the total solar eclipse of April 8, 2024. The search was conducted by a collaborative team of researchers from the University of Pittsburgh, Carnegie Mellon University, and Formant. Our team was one of those funded by NASA's Nationwide Eclipse Ballooning Program (NEBP) for the 2023 annular and 2024 total eclipses.

Shadow bands appear as rapidly moving, faint light and dark patterns on the ground just a few minutes before and after totality during a total solar eclipse [5, 8]. Typically reported to be about 10 cm apart, they form parallel lines that appear to shift dynamically as the eclipse progresses into and out of totality. Their existence is documented in historical records dating back to the 9th century CE [6]. Our team aimed to explore the underlying mechanisms of shadow bands, testing two competing theories: the Atmospheric Turbulence Theory and the Diffraction-Interference Theory.

The Atmospheric Turbulence Theory, introduced in detail by Codona in 1986 [2], attributes shadow bands to the disappearing crescent of sunlight rapidly refracted by atmospheric turbulence in the planetary boundary layer (PBL). In contrast, the Diffraction-Interference Theory suggests that these patterns arise above the atmosphere due to diffraction effects, possibly involving the Moon's disappearing bright limb or other effects [5]. To discriminate between these

theories, we utilized photodiode light sensors deployed on high-altitude balloons (HABs), similar ground based light sensors, and radiosondes launched on weather balloons to measure atmospheric turbulence. Additional data were collected with a plane-mounted light sensor. We were also prepared to make ground video observations.

Observations were primarily conducted in Concan, TX, within the path of totality, where maximum totality lasted over four minutes. Our instruments recorded light intensity and atmospheric conditions, and later spectrogram analysis searched for potential frequency signatures associated with shadow bands. Additional data from New Brunswick, Vermont, and New Hampshire supplemented our efforts.

Our study was built on the 2017 eclipse-balloon project conducted by the University of Pittsburgh, which identified a constant 4.5 Hz signal linked to shadow bands at an altitude of 25 km, well above the atmosphere's turbulent layer, as explained by Madhani et al. in 2020 [5]. However, despite deploying more sensitive sensors and extending the scope of measurements during the April 8 eclipse, we did not detect shadow bands with our HAB light sensors. But since our ground based light sensors in Concan were not operable due to clouds, it's possible that shadow bands were simply not present over Concan before and after totality. This research seeks to improve our understanding of the origins and characteristics of shadow bands, contributing to broader insights into atmospheric and optical phenomena observed during total eclipses.

The remainder of this paper is organized as follows. Section 2 describes the observations, including details of the totality path, the deployment of HABs with light sensors and weather balloons with radiosondes in Concan, and logs summarizing the data collection sessions. Section 3 provides a detailed explanation of our measurements and data processing methods, and outlines the data analysis leading to our results. Section 4 presents a discussion and summary of the findings, and suggestions for future research directions. An Appendix includes additional results in the form of Figures which researchers may find useful.

## 2. Observation and Data Collection

### 2.1. Instrumentation and Setup

Our research team employed a range of instruments to capture shadow band data.

Two HABs with 360-degree cameras, each equipped with two light sensors (designated as BL00, BL01, BL02, and BL03) sampling at 400 Hz, were launched in Concan and reached altitudes of 20 km and 25 km at the time of totality. These sensors provided sensitive data with negligible atmospheric distortion as the balloons were above the turbulent layer of the atmosphere. The area of the Hamamatus photodiodes used for this study was 12.96 mm<sup>2</sup>, which was slightly more than ten times the area of the Hamamatus photodiodes used in our 2017 study[5]. Our electronics were improved to minimize noise.

Light sensors were deployed on the ground at the launch site to measure fluctuations in light intensity. However, cloud cover during the eclipse made these data useless.

A total of 31 weather balloons carrying radiosondes were launched from Concan over a 30-hour period to measure temperature, pressure, wind speed, and humidity. These measurements allowed us to identify the height of the turbulent PBL near totality [4]. Launches occurred hourly beginning 24 hours before totality, with an additional launch during totality, and continued for six hours after totality.

Due to cloudy conditions in Concan, which discouraged us from attempting a flight near Concan, a light sensor was mounted on an aircraft flying at 3.6 km altitude in northeast Vermont, permitting us to collect additional relevant data above the turbulent PBL. Radiosonde data from a New Hampshire NEBP team confirmed that the PBL was below 2 km, suggesting that the aircraft sensor was operating above the turbulent layer. However, the separation between the plane and the New Hampshire radiosonde launches was about 80 km.

An excellent video of shadow bands was obtained in eastern New Brunswick, Canada, 540 km from the plane's flight path. This video confirmed the existence of shadow bands on the ground at that location, albeit 3500 km from our HAB light sensors above Concan and 540 km from our plane-mounted light sensor in northeast Vermont.

### 2.2. Observing Conditions

As noted, cloud cover in Concan hindered ground based measurements at the time of totality. Totality in Concan

took place from 18:30:13 to 18:34:37 UTC. Despite the clouds, the HAB light sensors provided excellent data, as the HABs remained above the cloud cover during the totality. Atmospheric conditions recorded by radiosondes indicated that the planetary boundary layer remained below 3 km, ensuring our HAB data were unaffected by low-level turbulence.

### 2.3. Data Processing and Measurement

All collected data were processed using Python. Light sensor data was recorded at approximately 400 Hz and analyzed using Fast Fourier Transform (FFT) spectrograms to detect frequency signatures indicative of shadow bands. Atmospheric measurements from radiosondes, including temperature, wind speed, and altitude were transmitted to ground station computers via a calibrated frequency, then downloaded as text files and processed using Python.

The radiosondes were not recovered, as their data transmission was sufficient for analysis. In contrast, data from the HABs required direct retrieval, necessitating our search team to locate and recover each HAB payload the day after launch. The HAB payloads were carefully balanced to minimize instances where the payload line interfered with the light sensor's line of sight to the eclipsed Sun. All light sensor data were stored as text files in voltage versus time format, providing records of light intensity variation versus time.

### 2.4. Observing Log

Data collection logs are presented in Table 1 for our light sensors and Table 2 for our radiosondes.

**Table 1**  
**Data Collection Log from Light Sensors**

Type	Location	Begin Date & Time (UTC)	End Date & Time (UTC)	<sup>1</sup> Area (mm <sup>2</sup> )	Altitude (km)	Comments
Ground GT00	Concan, TX	04/08/2024 17:42	04/08/2024 18:59	12.96	Ground level	Cloud cover
HAB BL00 + BL01	Concan, TX	04/08/2024 16:56	04/08/2024 17:53	12.96	25	Above PBL
HAB BL02 + BL03	Concan, TX	04/08/2024 16:30	04/08/2024 18:18	12.96	20	Above PBL
Aircraft	NE Vermont	04/09/2024 19:09	04/09/2024 19:40	12.96	3.6	Above PBL

<sup>1</sup>The photodiode area for this study was 12.96 mm<sup>2</sup>, whereas it was 1.21 mm<sup>2</sup> in our 2017 study[5], and our electronics were improved to minimize noise.

**Table 2**  
**Data Collection Log from Radiosondes Launched in Concan, TX**

Launch #	Location	Launch Date & Time (UTC)	Radiosonde Number (type and #)	Max Altitude (km)	Surface Temp (°C)	Full Flight	Reason if Not a Full Flight
01	Concan, TX	04/07/2024 18:18	DFM-17 22342-059024	32.606	25.3	Y	–
02	Concan, TX	04/07/2024 19:19	DFM-17 22353-059241	32.475	26.1	Y	–
03	Concan, TX	04/07/2024 20:18	DFM-17 22342-058813	32.769	27.7	Y	–
04	Concan, TX	04/07/2024 21:18	DFM-17 22342-058844	33.941	28.6	Y	–
05	Concan, TX	04/07/2024 22:20	DFM-17 22342-058776	33.010	29.2	N	Loss of Signal
06	Concan, TX	04/07/2024 23:18	DFM-17 22342-058897	35.045	28.2	Y	–
07	Concan, TX	04/08/2024 00:18	DFM-17 22342-058779	32.493	27.7	Y	–
08	Concan, TX	04/08/2024 01:18	DFM-17 22342-058906	12.818	24.5	N	Loss of Signal
09	Concan, TX	04/08/2024 02:18	DFM-17 22342-059023	32.210	21.0	Y	–
10	Concan, TX	04/08/2024 03:18	DFM-17 22342-059033	29.745	17.3	Y	–
11	Concan, TX	04/08/2024 04:18	DFM-17 22342-058915	26.185	16.1	Y	–
12	Concan, TX	04/08/2024 05:18	DFM-17 22342-058793	31.283	15.4	Y	–
13	Concan, TX	04/08/2024 06:18	DFM-17 22342-058902	34.363	17.0	Y	–
14	Concan, TX	04/08/2024 07:18	DFM-17 22353-059147	33.154	19.9	Y	–
15	Concan, TX	04/08/2024 08:18	DFM-17 22353-059218	32.967	20.6	Y	–
16	Concan, TX	04/08/2024 09:18	DFM-17 22353-059226	34.180	19.3	Y	–
17	Concan, TX	04/08/2024 10:18	DFM-17 22353-059209	34.602	19.3	Y	–
18	Concan, TX	04/08/2024 11:18	DFM-17 22353-059086	34.244	19.6	Y	–
19	Concan, TX	04/08/2024 12:18	DFM-17 22353-059227	33.583	19.7	Y	–
20	Concan, TX	04/08/2024 13:18	DFM-17 22342-0589954	31.486	19.8	Y	–
21	Concan, TX	04/08/2024 14:18	DFM-17 22342-058890	23.343	20.4	Y	–
22	Concan, TX	04/08/2024 15:18	DFM-17 22342-058892	32.733	20.7	Y	–
23	Concan, TX	04/08/2024 16:18	DFM-17 22342-058817	25.725	22.8	N	Ended Early for 25b
24	Concan, TX	04/08/2024 17:18	DFM-17 22342-058991	33.555	24.5	Y	–
25	Concan, TX	04/08/2024 18:18	DFM-17 22342-058815	29.705	23.8	Y	–
25b	Concan, TX	04/08/2024 18:26	DFM-17 22342-058958	30.495	23.7	Y	–
26	Concan, TX	04/08/2024 19:19	DFM-17 22353-059367	34.643	23.3	Y	–
27	Concan, TX	04/08/2024 20:18	DFM-17 22342-058886	33.209	23.1	Y	–
28	Concan, TX	04/08/2024 21:18	DFM-17 22342-058833	30.712	21.9	Y	–
29	Concan, TX	04/08/2024 22:18	DFM-17 22353-059080	32.743	24.0	Y	–
30	Concan, TX	04/08/2024 23:18	DFM-17 22353-059334	32.736	25.4	Y	–

### 3. Data Analysis

Data from the HABs, aircraft-mounted, and ground light sensors were analyzed in Python to search for shadow bands and, if present, determine their characteristics. Radiosonde data were also analyzed. This section explains the methodologies used to process and interpret the data.

#### 3.1. Spectrogram Analysis and Data Cleaning

Spectrograms were generated using FFT techniques, employing a Boxcar window function to analyze temporal frequency variations in the photodiode voltage data [1]. The Boxcar window was chosen over tapered windows (e.g., Hann) to avoid introducing artificial low-frequency harmonics that could be mistaken for shadow band behavior. Each spectrogram was computed using 5-second time segments with 50% overlap, yielding a frequency resolution of approximately 0.2 Hz. Power spectra were converted to decibels and visualized using intensity limits from  $-160$  dB to  $-20$  dB to enhance contrast and highlight faint, low-amplitude features of potential interest. These settings were selected to maximize sensitivity to frequency-domain signatures expected from shadow band oscillations.

Before spectrogram generation, the voltage time series were pre-processed to remove artifacts caused by payload line interference. These artifacts appeared as sharp, deep, and irregular voltage dips that were not physically meaningful and would otherwise dominate the spectrogram. To preserve the underlying eclipse light curve while eliminating artifacts, a multi-stage cleaning pipeline was implemented.

First, unrealistic voltage values outside the physical operating range of the photodiode were identified and replaced with `NaN` values to prevent their inclusion in subsequent smoothing operations. A bidirectional exponentially weighted moving average (EWMA) with a large span (1500 samples) was then used to estimate the global voltage trend throughout the flight. Deviations exceeding 0.10 V from this EWMA trend were classified as interference and removed. This threshold is significantly larger than the expected amplitude of physical shadow band fluctuations (0.03 V), ensuring that removal was limited to nonphysical artifacts while preserving genuine low-level signal variations.

A localized refinement step was applied to a short interval of the data containing exceptionally dense interference. Within this region, a smaller EWMA span and a relaxed deviation threshold (0.20 V) were used to more accurately isolate and restore the underlying eclipse curve. All removed values were subsequently reconstructed using linear interpolation within continuous segments to maintain smoothness in the cleaned light curve.

Finally, a second bidirectional EWMA smoothing pass was applied using the same global span to suppress any remaining small-amplitude irregularities while preserving the overall eclipse morphology. The result of this pipeline was a continuous, artifact-suppressed voltage series that retained both the eclipse profile and any physically meaningful temporal structure.

Figures 1–3 illustrate this full cleaning process for HAB BL00. Raw and cleaned voltage series are shown with their corresponding spectrograms. These same results are essentially identical to those from three other HAB photodiodes (BL01–BL03), as shown in Appendix Figures A1–A3. If shadow bands were present, they would appear as horizontal bands over a limited range of frequencies in the spectrograms. However, after cleaning, no persistent frequency signatures between 0.25 Hz and 100 Hz were detected from any of the HAB photodiodes, supporting the conclusion that shadow bands were absent at high altitudes over Concan.

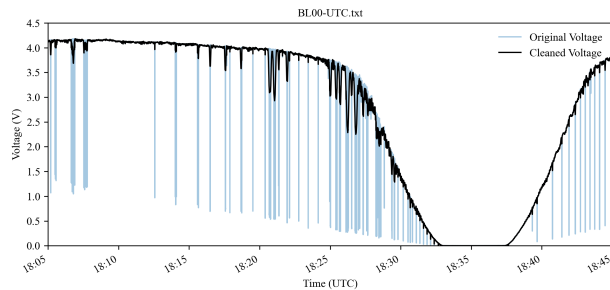


**Figure 1: Raw and cleaned light curve from the HAB BL00 photodiode sensor during the April 8, 2024, total solar eclipse.** The original signal (blue) includes sharp voltage dips caused by the payload line intermittently blocking the photodiode sensor. The cleaned signal (black) preserves the eclipse structure while removing these interference artifacts. Time is shown in UTC.

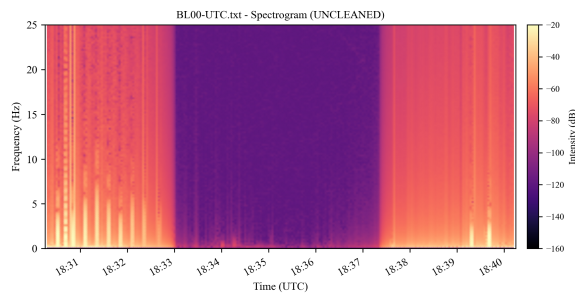


**Figure 2: Raw spectrogram of the HAB BL00 light intensity data during the April 8, 2024, total solar eclipse.** Spectrogram computed using a Fast Fourier Transform (FFT) with a 5-second boxcar window and 50% overlap. The shown frequency range spans 0–25 Hz. Intensity is shown in decibels (dB). No shadow band signal was detected.

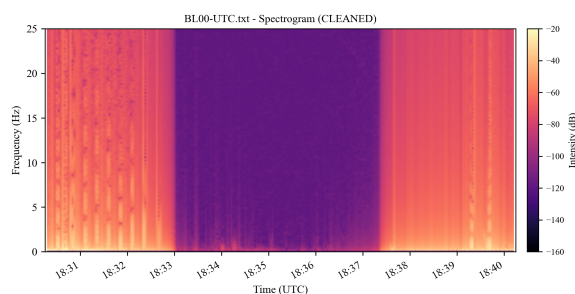


**Figure 3: Cleaned spectrogram of HAB BL00 light intensity data during the April 8, 2024, total solar eclipse.** The cleaning process partially removed voltage dips caused by intermittent payload line interference with the photodiode sensor. After cleaning, no shadow bands are detected. The spectrogram is free of distinct periodic signals up to 25 Hz (shown) and even up to 100 Hz (not shown).

### 3.2. Comparison of HAB, Aircraft, and Ground Data

After cleaning and generating the spectrograms, no periodic signals indicative of shadow bands were observed in the HAB BL00, BL01, BL02, and BL03 data (Figures 1–3, A1–A3). These consistent results, which include four independent high altitude light sensors, confirm that our removal of interference artifacts did not introduce artificial features or mask real oscillations in the frequency domain. Moreover, as noted in Section 2.1, the sensitivity and noise characteristics of our photodiodes was improved relative to our similar 2017 study. The lack of any persistent signatures between 0.25 Hz and 100 Hz indicates the absence of shadow bands at stratospheric altitudes above Concan.

Light sensor data were also collected from two other observational platforms: an aircraft-mounted one at 3.6 km altitude over northeast Vermont (Appendix Figure A4, designated PL00) and ground-based one in Concan (one of 14 is shown in Appendix Figure A5, designated GT00).

The aircraft served as an intermediate altitude platform, above the PBL, bridging the gap between HAB observations and ground-based measurements. Its spectrogram, computed without cleaning (as no payload interference artifacts were present), similarly revealed no shadow band frequencies (Appendix Figure A4).

Ground-based observations, however, were severely impacted by cloud cover during the eclipse. As a result, the spectrograms for the Concan ground sensors appear darker overall, with intermittent bright features corresponding to brief cloud clearings (Appendix Figure A5). These interruptions prevented any meaningful detection of oscillatory signals due to shadow bands on the ground in Concan.

There were various visual sightings of shadow bands on the ground along the eclipse path. Notably, video evidence of shadow bands was reported by an observer [7] in New Brunswick, Canada, approximately 3,500 km from Concan and 540 km from the aircraft flight path, confirming that shadow bands were present at some locations along the eclipse path (see video here). Our FFT analysis of the video from New Brunswick showed dominate frequencies at  $2.7 \pm 0.26$  Hz.

However, given the large separations between these various locations and possible differences in local atmospheric conditions, it is plausible that no shadow bands would have been visible on the ground in Concan or in northeast Vermont if it had been clear.

### 3.3. Atmospheric Turbulence and Shadow Bands

The PBL is the lowest region of the atmosphere, directly influenced by surface heating, turbulence, and mixing processes. It typically extends from the ground up to a few kilometers, with its height varying due to factors such as temperature gradients, wind shear, and solar radiation. The PBL plays a key role in atmospheric dynamics, as it is where most weather phenomena, including turbulence, occur.

Shadow bands have been theorized to originate from atmospheric turbulence within the PBL, which can create

rapid refractive distortions as light from the disappearing crescent Sun passes through density fluctuations in the air [2, 9]. Alternatively, diffraction-interference effects have also been proposed as an explanation for shadow band formation [5] and see [3].

To assess the role of turbulence for this study, our radiosonde data were analyzed to determine the height of the PBL during the eclipse. Temperature inversions, which indicate the location of stable air layers and the turbulent interface between the PBL and free atmosphere, were identified in the data. Wind shear measurements were also used to locate turbulence zones. The radiosonde data collected above Concan confirmed that the PBL remained below 3 km during totality (Figure 4; Flights 01, 25b, and 29).

Radiosonde profiles from New Hampshire provide additional context for conditions in the northeastern United States (Figure 5; Flights 02, 25, and 28). These profiles reveal a consistently shallow PBL, remaining just above 1 km near the time of the eclipse. Unlike from Concan, a radiosonde was not launched during totality in New Hampshire, but the flights bracket the eclipse period and collectively show stable boundary layer conditions with minimal vertical variability. These findings suggest that the aircraft-mounted light sensor, flying at an altitude of 3.6 km over Vermont, was likely positioned above the turbulent layer, ensuring that its measurements were unaffected by near-surface turbulence.

Thus, Figures 4 and 5, which show wind speed components and temperature profiles above Concan and New Hampshire, respectively, indicate that all optical measurements from the HABs and aircraft were collected well above the PBL, which isolated our searches for shadow bands from turbulence-induced variability within 3 km of the ground.

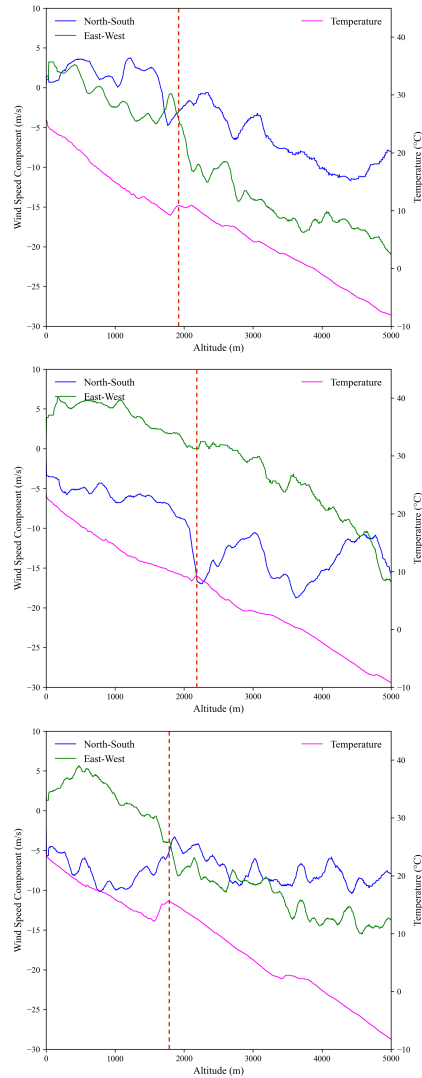


**Figure 4: Wind speed components and temperature profiles from radiosonde flights over Concan, TX.** **Flight 01** (Top) and **Flight 29** (Bottom) show that the PBL, characterized by temperature inversions and abrupt wind speed/direction changes, remains consistently below 3 km throughout all flights (all flights not shown). The vertical red dashed line highlights that the PBL is positioned between 1500 m and 2500 m. **Flight 25b** (Middle), which occurred during the total eclipse, exhibits a significant change in the north-south wind speed component in the same altitude range where a slight temperature inversion is observed, showing that the PBL is below 3 km during the eclipse.

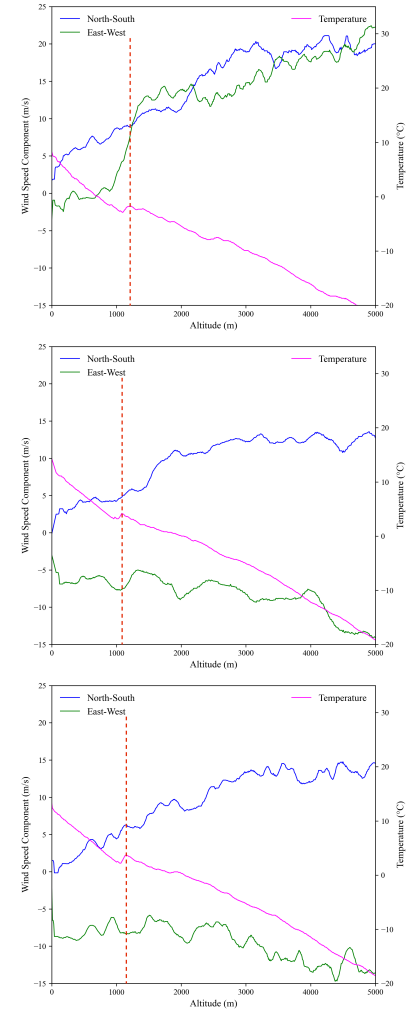


**Figure 5: Wind speed components and temperature profiles from radiosonde flights over New Hampshire.** **Flight 02** (Top) and **Flight 28** (Bottom) show a consistently stable PBL just above 1000 m, as indicated by the vertical red dashed line marking the location of temperature inversions. **Flight 25** (Middle), conducted closest to the time of the total eclipse, also shows a clear PBL inversion near this height as well. While no radiosonde was launched during totality, these flights provide a representative view of PBL conditions in the region. The stability of the PBL in these flights contrasts with the more variable PBL observed in Concan.

### 3.4. Comments on Artifacts and Challenges

During the data analysis, artifacts were identified that had to be removed from our HAB light sensor data. First, for example, obstruction from the payload line affected sensor readings, especially at higher altitudes where wind conditions were more likely to cause the payload to spin, but the spin was not periodic and of very low frequency. Also, additional low frequency intensity changes were due to payload movement.

Second, the radiosonde data collected above Concan was intended to be paired with ground based light sensor data to correlate atmospheric turbulence with light intensity fluctuations. However, cloud cover in Concan presented a challenge that did not allow us to realize this goal.

Third, in New Hampshire, where radiosonde data was also collected, we were unable to deploy ground based light sensors. This prevented a comparison between atmospheric turbulence and potential shadow band behavior at that location. This limitation of our study highlights the need for improved coordination between efforts to measure shadow bands above and below the PBL during future total solar eclipses.

## 4. Discussion and Summary

### 4.1. Discussion

The primary objective of this study was to determine whether shadow bands arise due to atmospheric turbulence or diffraction-interference effects. Despite deploying more advanced sensors and extending measurement locations beyond those used in 2017, no shadow bands were detected in the light sensor data collected by our HABs or aircraft. Our ground based light sensors were useless due to clouds.

Thus, there is a clear discrepancy between this 2024 study and our 2017 study. Our 2017 total solar eclipse shadow band data provided strong evidence for the diffraction-interference theory. Spectrogram analysis of light sensor data on both the ground in Tennessee and on a HAB at 25 km revealed a consistent 4.5 Hz signal which appeared before and after totality. This signal disappeared during totality but reappeared after totality, supporting the finding that this frequency was due to shadow bands. The 2017 balloon data were relatively clean, although they also contained artifacts at discrete times attributed to intermittent payload line interference. The 2017 ground data appeared to also contain chaotic frequencies due to atmospheric turbulence in addition to a 4.5 Hz signal. In contrast, the 2024 study failed to detect any signal between 0.25 Hz to 100 Hz were detected, despite the fact that we used more sensitive sensors with less noise. This raises questions about what atmospheric or geometric conditions lead to the appearance of shadow bands.

Several possibilities could explain the absence of shadow bands in 2024. One possibility is that shadow bands were not present at our high altitude observation sites due to some natural variability in their occurrence. Historical records indicate that shadow bands are not always observed near

totality, suggesting that their occurrence may depend on the observer's location within the path of totality or specific atmospheric conditions. It's unfortunate that cloud cover in Concan rendered our ground based light sensors ineffective, eliminating a crucial data source that could have confirmed their presence on the ground, which would have allowed us to reach a more firm conclusion.

The absence of shadow bands in our 2024 study challenges the conclusions of our 2017 study, which detected a persistent 4.5 Hz signal above the PBL and on the ground [5]. The signal detected in 2017 was robust in all of our light sensors, and it could not be reproduced in laboratory tests after the eclipse.

At the same time, given that the 2024 study utilized improved light sensors with larger surface areas and enhanced sensitivity, it is unlikely that shadow bands, if present, would have gone undetected. This discrepancy raises questions about whether the previously-observed signal was truly due to shadow bands or a different atmospheric or instrumental effect. The lack of ground based light sensor data or video data in New Hampshire and Vermont further limits our ability to draw conclusions. Future studies should prioritize deploying ground light sensors or sensitive video cameras at all sites where light sensors are deployed above the PBL. The use of radiosonde launches near totality would also be helpful to confirm the height of the PLB.

This study contributes to a broader understanding of eclipse-related optical phenomena by refining observational techniques and highlighting gaps in current methodologies.

### 4.2. Summary

This research investigated the presence and origin of shadow bands during the April 8, 2024, total solar eclipse. HAB and aircraft-mounted light sensors, and radiosondes were used. Unlike our 2017 eclipse study, which detected a 4.5 Hz signal attributed to shadow bands both on the ground and at an altitude of 25 km, no shadow bands were observed in 2024, even with improved instrumentation. Cloud cover prevented the use of ground based light sensors, limiting our ability to confirm whether shadow bands were also absent on the ground or merely undetectable due to the clouds.

A comparison between our 2017 and 2024 studies suggests two possible conclusions: (1) either shadow bands were not present in Concan and northeast Vermont during the 2024 eclipse or (2) our 2017 measurements were problematic. However, our 2017 data showed a clear 4.5 Hz signal before and after, but not during, totality, and the signal couldn't be reproduced in the lab after the 2017 eclipse. One possibility is that for shadow bands to be observable, either specific atmospheric conditions are required or specific but unknown diffraction-interference variables are required.

An important lesson learned is that it's not necessary to fly a HAB to very high altitudes to repeat this experiment. An aircraft flying above the turbulent PBL can accomplish the measurements. For future total eclipses, multiple coordinated measurements should be made above the PBL and ideally directly below on the ground.

Through improved experimental techniques and experience, this study contributes to the ongoing effort to understand the mechanisms which give rise to eclipse shadow bands.

## Acknowledgments

We thank Gary and Margaret Miller for flying their plane over northeast Vermont while one of us (JBP) pointed our PL00 light sensor at the eclipsed Sun. We thank Cliff Seruntine, who took the extraordinary video of shadow bands in East Brunswick, Canada. We thank and acknowledge Eric Kelsey and Genevieve Picciano, who made the New Hampshire radiosonde data available. And we thank Jerry Baker for his assistance with recovering a test flight payload. We gratefully acknowledge financial support from the NASA Nationwide Eclipse Ballooning Program, the NASA Space Grant Foundation, the NASA Pennsylvania Space Grant Consortium, and the University of Pittsburgh's Dietrich School, Frederick Honors College, Department of Physics and Astronomy, and Allegheny Observatory.

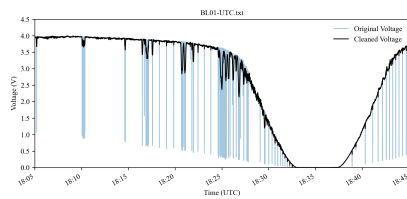
## References

- [1] Cerna, M., & Harvey, A. F. (2000). *The Fundamentals of FFT-Based Signal Analysis and Measurement*, Application Note 041, National Instruments.
- [2] Codona, J. L. (1986). A&A, 164, 415.
- [3] Elert, G. (2025). *Interference of Light*, The Physics Hypertextbook. Retrieved from <https://physics.info/interference-light/summary.shtml>
- [4] Li, H., Liu, B., Ma, X., Jin, S., Ma, Y., et al. (2021). Atmos. Meas. Tech., 14, 5977–5986. <https://doi.org/10.5194/amt-14-5977-2021>
- [5] Madhani, J., et al. (2020). J. Atmos. Solar-Terr. Phys., 211, 105420.
- [6] NASA. (2017). *Exploring Shadow Bands*. Retrieved from <https://eclipse2017.nasa.gov/exploring-shadow-bands>
- [7] Seruntine, C. (2024) [www.youtube.com/watch?v=1iqX6LPJKc](https://www.youtube.com/watch?v=1iqX6LPJKc)
- [8] Strickling, M. (n.d.). *Shadow Bands*. Retrieved from <https://www.strickling.net/shadowbands.htm>
- [9] Zhan, H., & Voelz, D. G. (2021). Appl. Opt., 60, 8426–8434.

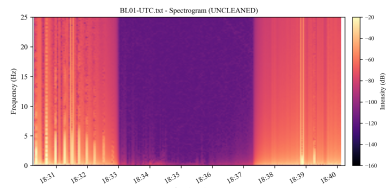
## A. Additional Light Curve and Spectrogram Results from other Light Sensors

For completeness, this Appendix includes full sets of light curves and spectrograms for all observational platforms. To make these figures, we used the same analysis and plotting procedures described in Section 3.1.

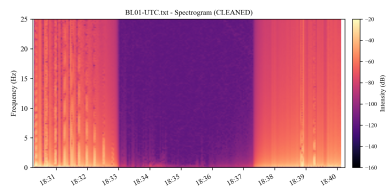
### Balloon Data (BL01–BL03)



(a) Light curve (cleaned)

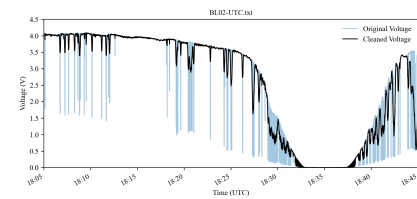


(b) Spectrogram (raw)

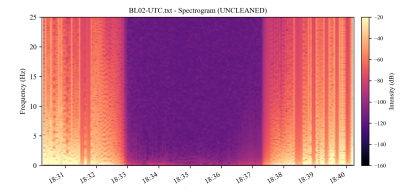


(c) Spectrogram (cleaned)

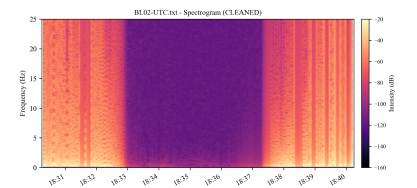
**Figure A1: Balloon BL01 data.** (a) Cleaned voltage versus time light curve, (b) corresponding raw spectrogram, and (c) corresponding cleaned spectrogram. The time interval shown for the light curve is larger than that shown for the spectrogram. The methods are the same as those described in Section 3.1.



(a) Light curve (cleaned)



(b) Spectrogram (raw)



(c) Spectrogram (cleaned)

**Figure A2: Balloon BL02 data.** (a) Cleaned voltage versus time light curve, (b) corresponding raw spectrogram, and (c) corresponding cleaned spectrogram. The time interval shown for the light curve is larger than that shown for the spectrogram. The methods are the same as those described in Section 3.1.

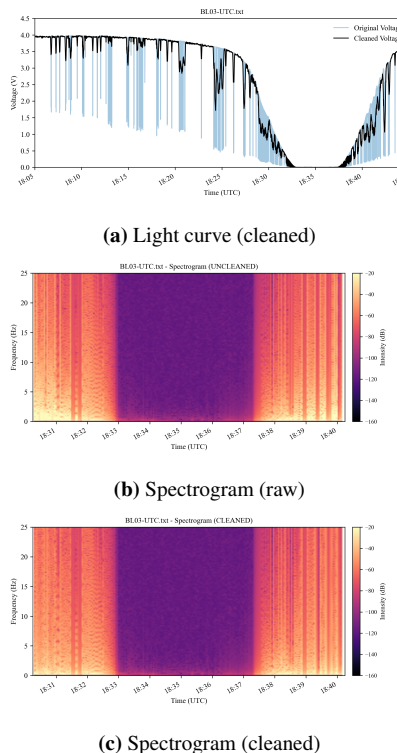
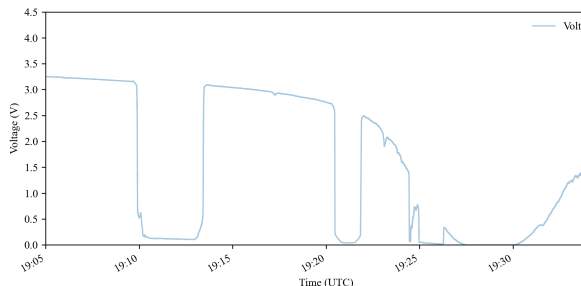
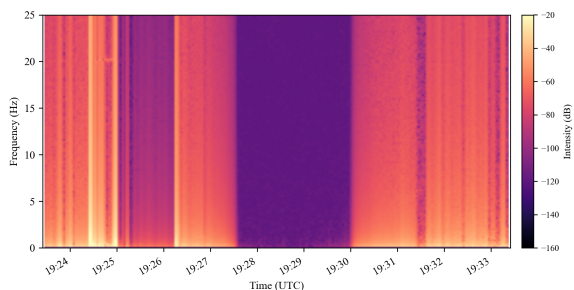


**Figure A3: Balloon BL03 data.** (a) Cleaned voltage versus time light curve, (b) corresponding raw spectrogram, and (c) corresponding cleaned spectrogram. The time interval shown for the light curve is larger than that shown for the spectrogram. The methods are the same as those described in Section 3.1.

**Aircraft Data (PL00)**



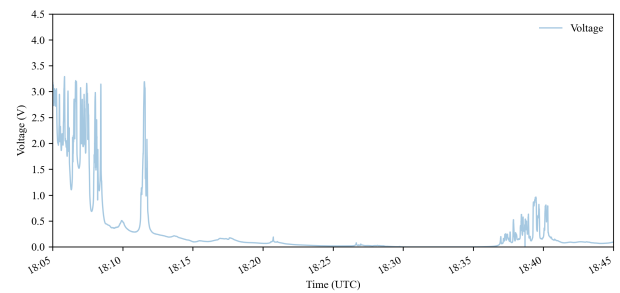
(a) Light curve



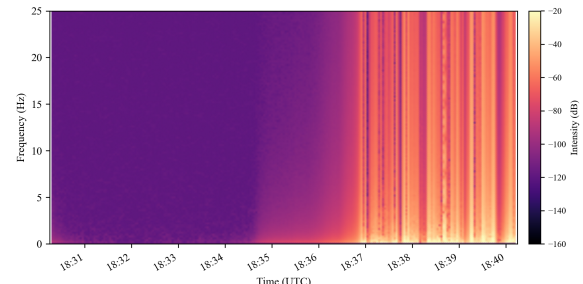
(b) Spectrogram

**Figure A4: Aircraft-mounted light sensor (designated PL00).**  
 (a) Voltage versus time light curve and (b) spectrogram computed using a 5-second Boxcar window with 50% overlap. The time interval shown for the light curve is larger than that shown for the spectrogram. Drops in the light curve occurred when the PL00 photodiode was not pointing toward the Sun to reposition it. Data cleaning was not applied since payload interference artifacts were not present. The methods are described in Section 3.1.

## Ground Array Data (GT00)



(a) Light curve



(b) Spectrogram

**Figure A5: Ground array light sensor (designated GT00, which was one of 14 ground light sensors).** (a) Voltage versus time light curve and (b) spectrogram computed using a 5-second Boxcar window with 50% overlap. Any meaningful analysis was limited by cloud cover during totality, as discussed in Section 3.2.